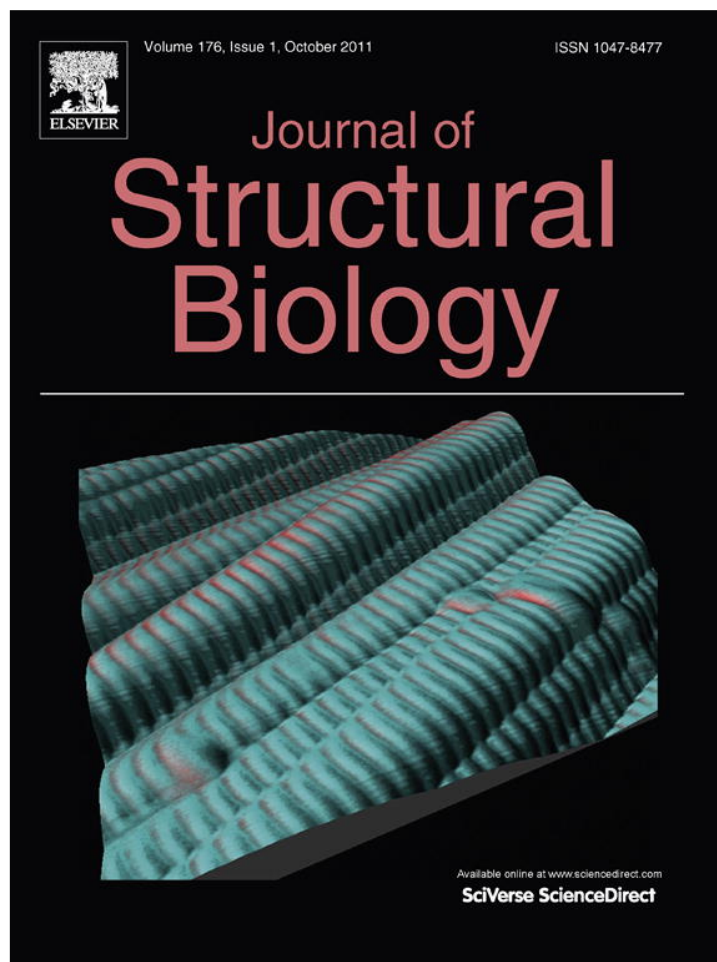


Provided for non-commercial research and education use.
Not for reproduction, distribution or commercial use.



This article appeared in a journal published by Elsevier. The attached copy is furnished to the author for internal non-commercial research and education use, including for instruction at the authors institution and sharing with colleagues.

Other uses, including reproduction and distribution, or selling or licensing copies, or posting to personal, institutional or third party websites are prohibited.

In most cases authors are permitted to post their version of the article (e.g. in Word or Tex form) to their personal website or institutional repository. Authors requiring further information regarding Elsevier's archiving and manuscript policies are encouraged to visit:

<http://www.elsevier.com/copyright>



Contents lists available at ScienceDirect

Journal of Structural Biology

journal homepage: www.elsevier.com/locate/yjsbi

Structural insights into the cofactor-assisted substrate recognition of yeast quinone oxidoreductase Zta1

Peng-Chao Guo, Xiao-Xiao Ma, Zhang-Zhi Bao, Jin-Di Ma, Yuxing Chen, Cong-Zhao Zhou *

Hefei National Laboratory for Physical Sciences at Microscale and School of Life Sciences, University of Science and Technology of China, Hefei Anhui 230027, People's Republic of China

ARTICLE INFO

Article history:

Received 17 May 2011

Received in revised form 14 July 2011

Accepted 19 July 2011

Available online 26 July 2011

Keywords:

Quinone oxidoreductases

Saccharomyces cerevisiae

Crystal structure

Substrate-binding pocket

Substrate specificity

Enzymatic kinetics

ABSTRACT

Quinone oxidoreductase (QOR *EC*1.6.5.5) catalyzes the reduction of quinone to hydroxyquinone using NADPH as a cofactor. Here we present the crystal structure of the ζ -crystallin-like QOR Zta1 from *Saccharomyces cerevisiae* in apo-form at 2.00 Å and complexed with NADPH at 1.59 Å resolution. Zta1 forms a homodimer, with each subunit containing a catalytic and a cofactor-binding domain. Upon NADPH binding to the interdomain cleft, the two domains shift towards each other, producing a better fit for NADPH, and tightening substrate binding. Computational simulation combined with site-directed mutagenesis and enzymatic activity analysis defined a potential quinone-binding site that determines the stringent substrate specificity. Moreover, multiple-sequence alignment and kinetics assays implied that a single-residue change from Arg in lower organisms to Gly in vertebrates possibly resulted in elevation of enzymatic activity of ζ -crystallin-like QORs throughout evolution.

© 2011 Elsevier Inc. All rights reserved.

1. Introduction

Most quinones are generally classified as toxic compounds that are widely distributed in nature. Cellular accumulation of quinones leads to serious cytotoxic effects in various ways (Bolton et al., 2000). Quinone dehydrogenase/oxidoreductases protect cells from the cytotoxic effects of quinones (Dinkova-Kostova and Talalay, 2000; Nioi and Hayes, 2004; Porte et al., 2009a). These enzymes catalyze the reduction of quinone to its corresponding hydroquinone, which is readily conjugated to either glucuronic acid or sulfate for excretion (Monks and Jones, 2002; Prestera et al., 1993).

NADPH-dependent quinone oxidoreductases (QORs, *EC* 1.6.5.5) belong to the nonmetallic reductase subfamily of the medium-chain dehydrogenase/reductase superfamily, which contains enzymes widespread in bacteria and eukaryotes (Porte et al., 2009a). The soluble QORs are distinct from the membrane-bound ones which are NADH-dependent, and contain noncovalently bound FMN and iron-sulfur clusters as prosthetic groups (Yagi, 1991). They are also different from the widely distributed quinone dehydrogenases (*EC* 1.6.5.2) that catalyze two-electron reductions and require FAD as an additional prosthetic group (Jaiswal, 2000; Li et al., 1995). The ζ -crystallins are NADPH-dependent QORs that were first identified

Abbreviations: QOR, quinone oxidoreductase; NQ, 1,2-naphthoquinone; PQ, 9,10-phenanthrenequinone.

* Corresponding author. Fax: +86 551 3600406.

E-mail address: zcz@ustc.edu.cn (C.-Z. Zhou).

1047-8477/\$ - see front matter © 2011 Elsevier Inc. All rights reserved.

doi:10.1016/j.jsb.2011.07.010

in the lenses of guinea pigs (Huang et al., 1987) and camels (Garland et al., 1991). Initially, Rao et al. reported that ζ -crystallins catalyze one-electron reduction of *ortho*-quinone (Rao et al., 1992). However, recent investigation showed that QORs catalyze two-electron reduction to convert quinone to its corresponding reduced quinone using NADPH as a cofactor (Oppermann, 2007; Porte et al., 2009b). The ζ -crystallin-like QORs have also been found in other organisms. *Pseudomonas syringae* pv. *tomato* DC3000 encodes a ζ -crystallin-like QOR that possesses a weak reduction activity towards 1,4-benzoquinone, and very strong activity towards 9,10-phenanthrenequinone (Pan et al., 2009). Human ζ -crystallin (Fernandez et al., 2007) and QorA from *Staphylococcus aureus* (Maruyama et al., 2003) catalyze the reduction of *ortho*-quinone.

To date, the structures of human ζ -crystallin (Porte et al., 2011), its homologs from *Escherichia coli* (Thorn et al., 1995), and *P. syringae* pv. *tomato* DC3000 (Pan et al., 2009) have been determined. All exist as a homodimer in the asymmetric unit, with each subunit composed of a catalytic domain and a cofactor-binding domain. The catalytic domain contains both the N- and C-termini of the protein and has a complex arrangement of secondary structures. The cofactor-binding domain exhibits two repetitive classic Rossmann folds (Rao and Rossmann, 1973). The ζ -crystallin-like QORs have been biophysically and structurally characterized. However, little is known about their substrate-binding site and catalytic mechanism.

The homolog of ζ -crystallin in *Saccharomyces cerevisiae* is Zta1, and it localizes in both the cytoplasm and the nucleus (Porte et al., 2009a). Zta1 is reported to have a similar substrate specificity

to human (Fernandez et al., 2007) and guinea pig ζ -crystallins (Rao et al., 1992). In addition to the detoxification of quinones, Zta1 and human ζ -crystallin also have the ability to reduce the α,β -double bond of alkenals/ones (Crosas et al., 2011; Porte et al., 2011), and involve in posttranscriptional regulation via binding to specific RNA sequences (Fernandez et al., 2007; Tang and Curthoys, 2001). Here, we determined the crystal structures of Zta1, in the apo-form at 2.00 Å and complexed to NADPH at 1.59 Å. The structures enabled us to identify a noticeable induced fit upon NADPH binding. We also defined a substrate-binding site using computational simulation and enzymatic activity assays. Furthermore, we found that a change in a single residue at the gate of the substrate-binding pocket might cause elevation of enzymatic activity of ζ -crystallin-like QORs from lower to higher organisms.

2. Materials and methods

2.1. Construction, expression, and purification of Zta1

The open reading frame of *ZTA1/YBR046C* was amplified by PCR, using *S. cerevisiae* S288c genomic DNA as the template, and cloned into a pET28a-derived vector. This construct adds a hexahistidine-tag to the N-terminus of the recombinant protein, which was over-expressed in *E. coli* BL21 (DE3) (Novagen, Madison, WI) strain using 2 × YT culture medium. The cells were induced with 0.2 mM isopropyl- β -D-thiogalactoside (IPTG) at 16 °C for 20 h when OD_{600nm} reached 0.6. Cells were harvested by centrifugation at 8000g for 10 min and resuspended in lysis buffer (20 mM Tris-HCl, pH 7.0, 200 mM NaCl). After 5 min of sonication and centrifugation at 12,000g for 25 min, the supernatant containing the soluble target protein was collected and loaded to a Ni-NTA column (GE Healthcare) equilibrated with binding buffer (20 mM Tris-HCl, pH 7.0, 200 mM NaCl). The target protein was eluted with 250 mM imidazole buffer and further loaded onto a Superdex 200 column (GE Healthcare) equilibrated with 20 mM sodium citrate, pH 5.38, 50 mM NaCl. Fractions containing the target protein were pooled and concentrated to 20 mg/mL. The purity of protein was estimated on SDS-PAGE and the protein sample was stored at -80 °C. The mutant proteins were expressed, purified, and stored in the same manner as the wild-type protein.

2.2. Crystallization, data collection, structure solution, and refinement

Crystals of Zta1 were obtained at 289 K using the hanging drop vapor-diffusion techniques, with the initial condition by mixing 1 μ L of the 20 mg/mL protein sample with equal volume of mother liquor (25% polyethylene glycol 3350, 0.2 M MgCl₂, 0.1 M Tris-HCl pH 8.0). The crystals grew to approximately 0.2 × 0.2 × 0.4 mm in about 3 days. Crystals of Zta1-NADPH complex were obtained by co-crystallizing Zta1 with 5 mM NADPH in 25% polyethylene glycol 3350, 0.1 M Tris-HCl pH 8.0. The crystals were soaked into the cryoprotectant of reservoir solution supplemented with 25% glycerol and flash-cooled at 100 K in liquid nitrogen, data were collected at radiation wavelength of 0.9795 Å at the Shanghai Synchrotron Radiation Facility, Shanghai Institute of Applied Physics, Chinese Academy of Sciences, using beamline BL17U at 100 K with a MX-225 CCD (Marresearch). Data processing and scaling were performed using the HKL2000 package (Otwinowski and Minor, 1997). Both crystal structures were determined by the molecular replacement method with *MOLREP* (Vagin and Teplyaev, 1997) using the coordinates of *E. coli* QOR in complex with NADPH (PDB code: 1QOR) as the search model. Refinement was carried out using *REFMAC* (Murshudov et al., 1997) and *Coot* (Emsley and Cowtan, 2004). The overall assessment of model quality was performed using *MolProbity* (Lovell et al., 2003). The

crystallographic parameters of the structures are listed in Table 1. All structure figures were prepared with *PyMOL* (DeLano, 2002).

2.3. Computational docking

The three dimensional structures of NQ and PQ were transformed with the program *phnix.elbow* (Adams et al., 2002) from the simplified molecular input line entry specification (SMILES) level representations (O = C1C = CC2 = C(C = CC = C2)C1 = O) and (O = C1C(=O)C2 = C(C = CC = C2)C3 = C1C = CC = C3). Enzyme structures for docking were prepared with *AutoDock Tools*, and docking runs were performed using *AutoDock4.0* (Goodsell et al., 1996; Huey et al., 2007). Up to 100 initial poses per molecule were generated, for each of which multiple conformations were scored. The best scoring pose was rigid-body minimized and scored for electrostatic and van der Waals interactions.

2.4. Enzymatic activity assay

The enzymatic kinetic parameters of native Zta1 and its mutants were measured as previously described (Rao et al., 1992) with minor changes. All assays were performed at 25 °C in a standard assay mixture contained 100 mM Tris-HCl, pH 7.5, 0.2 mM NADPH, purified protein and substrates at various concentrations. Quinone substrates were dissolved in absolute alcohol (final concentration of alcohol in assay was 2%). The reactions were triggered by adding the purified protein solution, and the decrease in absorbance at 340 nm ($\epsilon_{\text{NADPH}} = 6220 \text{ M}^{-1} \text{ cm}^{-1}$) was monitored with a DU800 spectrophotometer (Beckman Coulter) equipped with a cuvette holder fixed at 25 °C. The decrease of absorbance resulting

Table 1
Data collection and refinement statistics.

	Apo-form	NADPH-bound form
<i>Data collection</i>		
Space group	P2 ₁ 2 ₁ 2 ₁	P2 ₁
Unit cell (Å, °)	74.97, 87.31, 100.51	53.96, 75.36, 182.83
	90, 90, 90	90, 92.11, 90
Molecules per asymmetric unit	2	4
Resolution range (Å) ^a	50.00–2.00 (2.07–2.00)	50.00–1.59 (1.62–1.59) ^a
Unique reflections	45,227 (4464)	190,318 (8502)
Completeness (%)	100.0 (100.0)	97.2 (87.4)
<I/σ(I)>	22.90 (7.73)	8.68(6.05)
R _{merge} ^b (%)	8.5 (27.6)	10.6 (15.7)
Average redundancy	6.2	3.5
<i>Structure refinement</i>		
Resolution range (Å)	35.32–2.00 (2.05–2.00)	35.50–1.59 (1.63–1.59)
R-factor ^c /R-free ^d (%)	21.4/24.7	18.8/21.1
Number of protein atoms	5190	10340
Number of water atoms	721	1627
RMSD ^e bond lengths (Å)	0.006	0.014
RMSD bond angles (°)	0.887	1.280
Mean B factors (Å ²)	19.6	16.7
<i>Ramachandran plot</i> ^f		
Most favored (%)	99.2	99.5
Additional allowed (%)	0.8	0.5
PDB entry	3QWA	3QWB

^a Values in parentheses are for the highest resolution shell.

^b $R_{\text{merge}} = \frac{\sum_{hkl} \sum_i |I_i(hkl) - \langle I(hkl) \rangle|}{\sum_{hkl} \sum_i I_i(hkl)}$, where $I_i(hkl)$ is the intensity of an observation and $\langle I(hkl) \rangle$ is the mean value for its unique reflection; Summations are over all reflections.

^c R-factor = $\frac{\sum_{hkl} ||F_o(h)| - |F_c(h)||}{\sum_{hkl} |F_o(h)|}$, where F_o and F_c are the observed and calculated structure-factor amplitudes, respectively.

^d R-free was calculated with 5% of the data excluded from the refinement.

^e Root-mean square-deviation from ideal values.

^f Categories as defined by *MolProbity*.

from the non-enzymatic reduction of quinone substrates upon addition of NADPH was set as background control for each assay.

3. Results and discussion

3.1. Overall structure

The two subunits in the asymmetric unit of the Zta1 crystal are structurally similar, with an overall root mean square deviation (RMSD) of 0.7 Å over 330 C α atoms. The subunits form a homodimer along a noncrystallographic 2-fold axis, with an interface of 1200 Å² (Fig. 1A). Gel-filtration chromatography indicated that Zta1 also exists as a dimer in solution (Fig. S1). The dimeric interface is mainly composed of strand β 13, helix α 8, and three loops (Pro255–Ile258, Ser262–Ile266 and Arg270–Gln272) in each monomer. Across the dimeric interface, the six-stranded parallel β -sheets of the two subunits form an extended β -sheet with β 13 and β 13' antiparallel.

Each Zta1 subunit is characterized by two distinct domains: a catalytic domain (Domain I) and a cofactor-binding domain (Domain II), which are bridged by a long helix α 3 (Fig. 1B). Domain I comprises an N-terminal segment (from Ile5 to Gln132) and a C-terminal segment (from Leu273 to Gln334), and forms a twisted β -sheet flanked by six α -helices (α 1, α 2, α 3a, and α 9– α 11). Domain II is from Val1133 to Gln272, and contains two repetitive Rossmann folds (Rao and Rossmann, 1973): β 8– α 4– β 9– α 5– β 10 and β 11– α 7– β 12– α 8– β 13. The six β -strands (β 8– β 13) form a central parallel β -sheet sandwiched by α -helices (α 3b– α 8).

3.2. NADPH-binding site and induced fit

A molecule of NADPH binds to the cleft between Domain I and II in each subunit of NADPH-complexed Zta1 (Fig. 1B and Fig. S2A), similar to previous complex structures (Porte et al., 2011; Thorn

et al., 1995). Superposition of the Zta1–NADPH monomer with the *Homo sapiens* and *E. coli* homologs yields an RMSD of 2.5 Å (282 C α atoms) and 1.4 Å (280 C α atoms), respectively.

The NADPH molecule at the interdomain cleft interacts with residues from both domains (Fig. 2A). The NADPH adenine ring is sandwiched between the main chains of Ala249 and Ser250 and the side chains of Phe49 and Arg322 via van der Waal's contacts. The amino group of the adenine moiety is exposed to solvent. The phosphate group of the adenosine ribose forms four hydrogen bonds with Ser181–N and O γ , Lys185–N ζ and Arg322–N η 2. The pyrophosphate fits into the relatively narrow part of the cleft, and forms hydrogen bonds with the main-chain atoms of Tyr49, Gly160 and Val161, and with Gln132–N ϵ 2. The two hydroxyl groups of the nicotinamide ribose are stabilized by Tyr53–O η via two hydrogen bonds. The nicotinamide moiety fits into a wider cavity and forms hydrogen bonds with Phe246–O, Pro271–O, and Leu273–N. A cluster of hydrogen bonds mediated by 13 water molecules in the NADPH-binding cleft further strengthen the protein-cofactor interaction.

Superposition of the apo-form against the NADPH-complexed Zta1 yields an RMSD of 1.2 Å over 325 C α atoms, and reveals conformational change induced by NADPH binding. Given Domain II superimposed first, Domain I shifts toward NADPH, resulting in helix α 3 rotating about 5.6° along its C-terminus. The rigid-body rotation of Domain I leads to a narrower interdomain cleft for the approaching NADPH molecule (Fig. S2B). The phenolic rings of Tyr49 and Tyr53 also shifted by about 3.2 and 3.4 Å to stabilize the adenosine ribose and pyrophosphate of NADPH. The short helix α 8' (Asn248–Gly251) is relaxed into a loop that packs against NADPH. The side chain of Arg322 shifts about 6.5 Å towards the phosphate group, leaving room for the NADPH adenine moiety.

In some liver alcohol dehydrogenases (Colonna-Cesari et al., 1986; Eklund et al., 1981), NADPH binding also results in a narrowing of the cofactor-binding cleft, and the active site is shielded from the solution. However, NADPH binding causes the opening of the

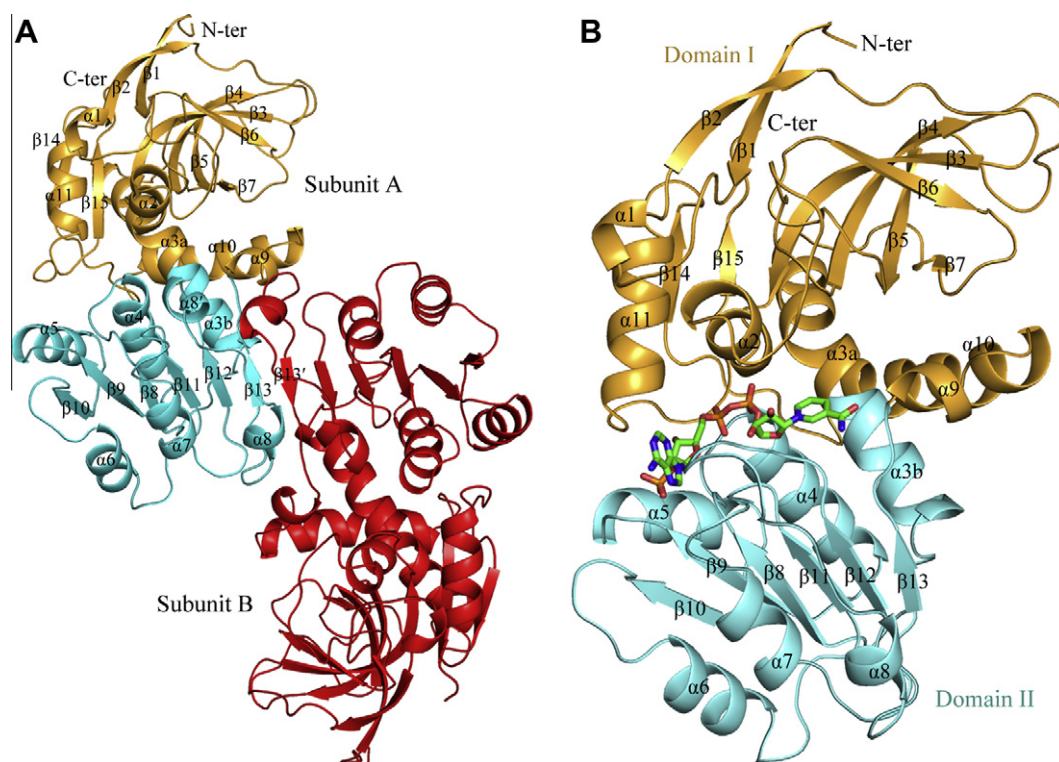


Fig. 1. Overall structure. (A) Schematic representation of the Zta1 dimer. (B) Cartoon representation of the Zta1–NADPH complex monomer. Orange, domain I; cyan, domain II. All figures were prepared using PyMOL.

interdomain cleft in *P. syringae* pv. *tomato* DC3000 QOR(Pan et al., 2009), and triggers no induced fit in *Thermus thermophilus* HB8 QOR(Shimomura et al., 2003).

3.3. Substrate-binding pocket

Upon NADPH binding, a group of residues undergo significant conformational changes (Fig. 2B). For example, Asn48, Ile50, Tyr53, and Tyr59 shift by 1.6, 5.4, 3.4, and 3.6 Å, respectively. The main chains of Arg69 and Asn248 shift towards the nicotinamide ring, together with the side chains reorienting by 6.0 and 4.7 Å. The side chains of Leu131, Arg270, Gln272, and Leu273 are shifted by about 3.8, 1.5, 5.6, and 0.5 Å, respectively. These residues, together with the nicotinamide ring, form a substrate-binding pocket, as proposed previously (Porte et al., 2009a; Thorn et al., 1995). Two hydrophobic sidewalls are composed of Ile50 and Tyr59 on one side, and the nicotinamide ring and Leu273 on the other side, while the hydrophilic sidewalls consist of Asn48, Asn248, Arg270 and Gln272. In addition, a glycerol was found in the substrate-binding pocket (Fig. 2A), held tightly in place by hydrogen bonds to the protein and NADPH molecule.

3.4. Putative binding sites of NQ and PQ in the substrate-binding pocket

We attempted to obtain the crystal of Zta1 tertiary complex with NADP⁺ and *ortho*-quinone by either co-crystallization or crystal soaking, but were not successful. Therefore, we docked two typical *ortho*-quinone substrates, 1,2-naphthoquinone (NQ) or 9,10-phenanthrenequinone (PQ), to the Zta1–NADPH complex using the program AutoDock4.0 (Huey et al., 2007; Morris et al., 1998). Docking produced nine clusters for NQ and five for PQ. Results for each substrate contained two clusters of lowest energy that satisfied the best interaction restraints. All quinone rings of the four probable clusters packed in parallel to the nicotinamide ring. However, the two most probable clusters for each substrate had two opposite positions, with the carbonyl groups of quinone either pointing towards Tyr59, Arg270, and Gln272 (outward pose, Fig. S3A and S3B), or toward Asn48 (inward pose, Fig. 3A and B). To verify the docking results, a series of residues involved in substrate binding (Ile50, Tyr59, Leu131, Arg270, Gln272, Leu273, and Asn48) were mutated for activity assays.

We measured the activity of the mutants of Ile50, Tyr59, Leu131, and Leu273, which are predicted to stabilize the phenyl rings of the substrate in either pose. As shown in Fig. 4A and B and Table S1, the K_m values for mutant Y59A towards both substrates were about 2-fold higher than wild-type, while the K_m^{NQ} value of Y59F changed little and K_m^{PQ} value decreased by 4-fold. The K_m for I50A towards both substrates, and the K_m^{PQ} of L131A were significantly increased, while the K_m^{NQ} for L131A, and the K_m for L273A towards both substrates showed little change. These results indicated that residues Ile50, Tyr59, and Leu131 are involved in substrate binding, although Leu131 is probably involved in immobilizing only the larger ring of PQ, but not NQ. Moreover, the k_{cat} values of mutants L131A and L273A towards both substrates decreased by 20–40% compared to wild-type, implying that these two residues are essential for shaping a hydrophobic environment around the C4 atom of NADPH for facilitating electron transfer.

We next measured the activity of the mutants of Tyr59, Arg270, and Gln272, which were predicted to form hydrogen bonds with the carbonyl groups of quinone in the outward pose. The K_m for R270A and Q272A towards both substrates, and the K_m^{NQ} of Y59F changed little compared to wild-type, whereas K_m^{PQ} for Y59F decreased by 4-fold. Moreover, electron transfer from C4 of the nicotinamide to carbonyl oxygen was not geometrically feasible in the outward pose. Thus, neither NQ nor PQ as substrate appeared to adopt an outward pose in the pocket. In contrast, the K_m^{NQ} and K_m^{PQ} for mutant N48A and N48L increased by more than 10-fold, while the k_{cat}^{NQ} and k_{cat}^{PQ} decreased by about 90% compared to wild-type, implying that Asn⁴⁸ is crucial for substrate stabilization and catalytic reaction.

Taken together, these results indicated that the inward pose (Fig. 3A and B) probably resembles the natural binding of the *ortho*-quinones: one carbonyl oxygen atom interacts with the side chain of Asn48 through a hydrogen bond (about 3.9 Å), and the other lies on top of the C4 atom of the nicotinamide (about 3.3 Å). Thus, we deduced that the re-distribution of hydrophobic and polar residues in the pocket upon NADPH binding creates an ideal environment for accommodating both the hydrophobic and polar moieties of the *ortho*-quinones.

Moreover, multiple-sequence alignment shows the active-site residues Asn48, Ile50, Tyr59, Leu131, and Leu273 are conserved in the typical ζ -crystallin-like QORs (Fig. 5A) and possess a common substrate-binding pattern that is distinct from other QOR

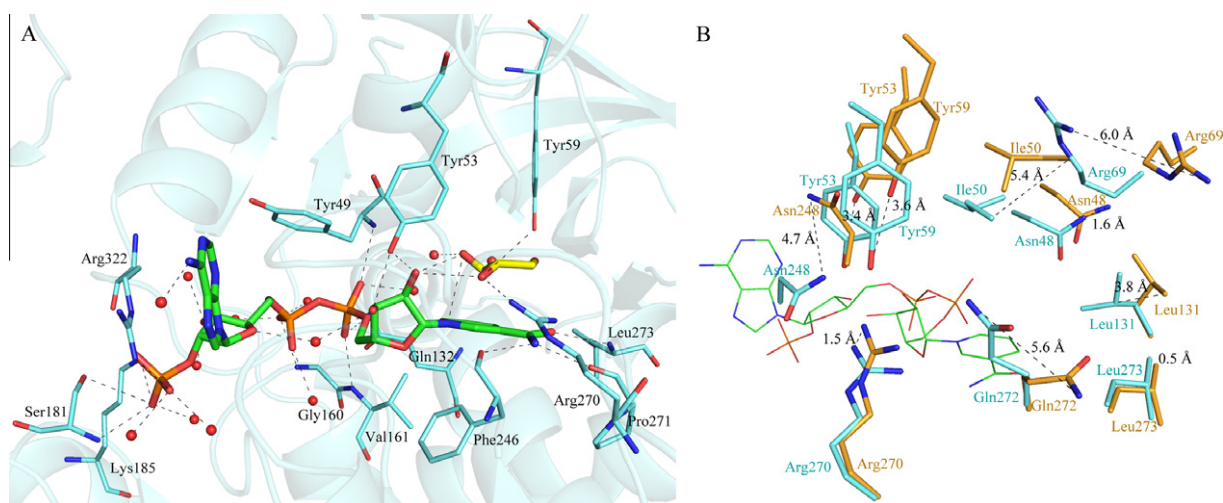


Fig. 2. NADPH binding. (A) Hydrogen bonds between NADPH and surrounding residues and waters are black dashed lines. NADPH, glycerol and surrounding residues are sticks, and waters are red spheres. (B) Superposition of residues in the substrate-binding pocket. Orange, Zta1; cyan, Zta1–NADPH complex; green NADPH. (For interpretation of the references to colour in this figure legend, the reader is referred to the web version of this article.)

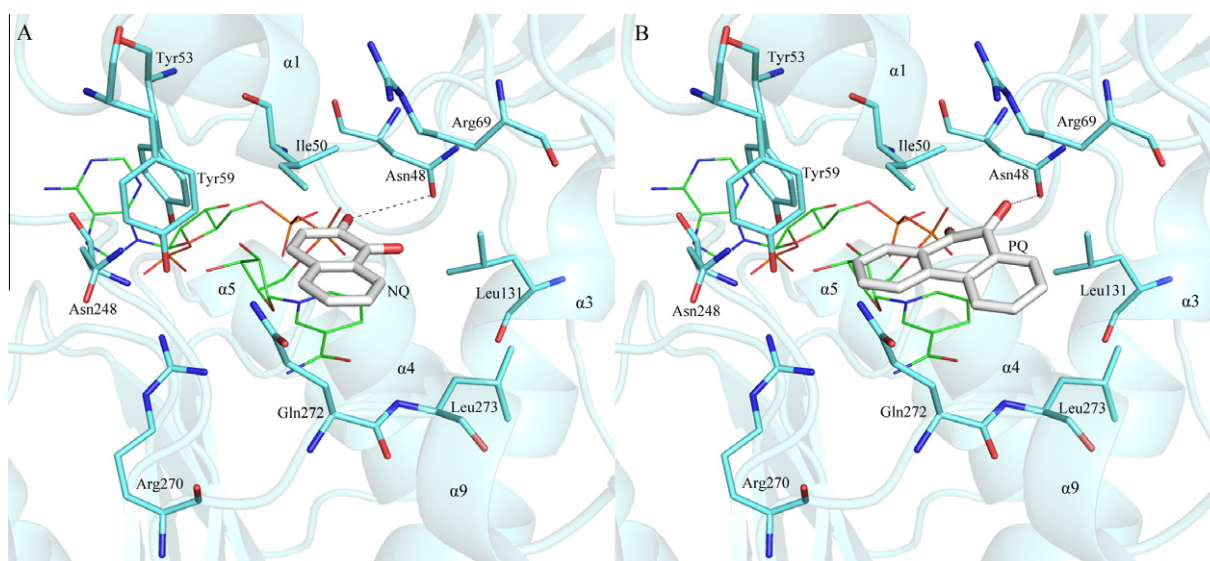


Fig. 3. Docking of NQ and PQ to Zta1. Binding pattern of (A) NQ and (B) PQ to the Zta1 active site. Residues are shown in cyan stick format. NADPH is green, and docked NQ and PQ are gray. Hydrogen bonds between the residues and docked quinones are black dashes. (For interpretation of the references to colour in this figure legend, the reader is referred to the web version of this article.)

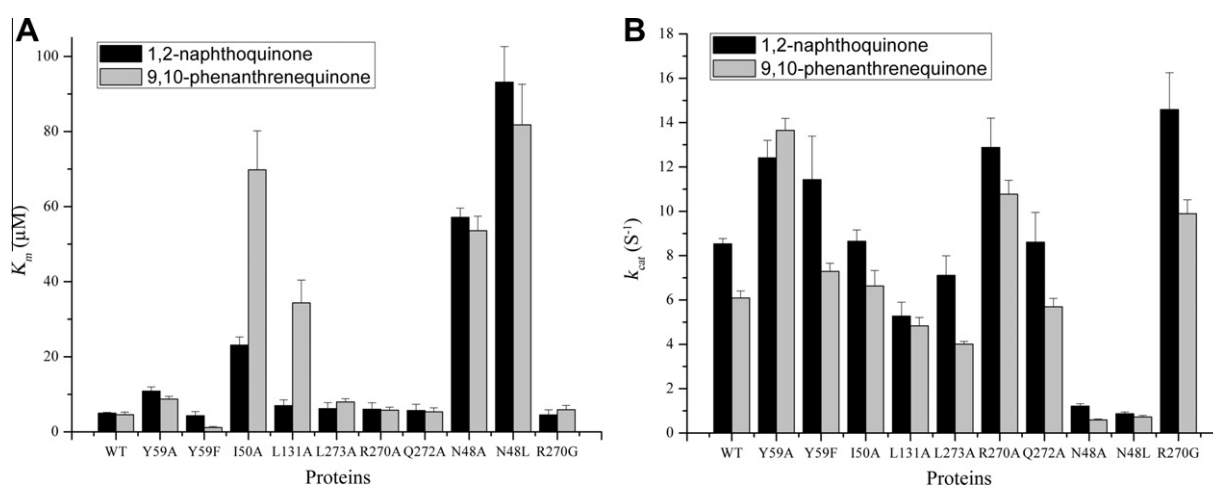


Fig. 4. The bar graph diagrams of kinetic parameters. (A) k_m and (B) k_{cat} value of mutants toward both substrates were compared with those of wild-type.

subfamilies (Porte et al., 2009a). For instance, the active site of *Thermus thermophilus* HB8 QOR (Shimomura et al., 2003) differs markedly from Zta1 and *E. coli* QOR, which belong to the typical ζ -crystallin-like QORs. This structural feature explains why *T. thermophilus* QOR has reductase activity towards 1,4-benzoquinone but not NQ or PQ. The conserved hydrophobic residue Leu131 in the typical ζ -crystallin-like QORs changes to Glu123 in all p53-inducible gene 3 (PIG3) members (Porte et al., 2009b), which consistent with their distinct substrate specificity. In addition, Zta1 and human ζ -crystallin have been reported to be able to reduce the α , β -double bond of alkenals/ones, using Tyr53 and Tyr59 as catalytic residues, alternatively (Crosas et al., 2011; Porte et al., 2011).

3.5. A single-residue change possibly contributes to elevate the enzymatic activity of ζ -crystallin-like QORs

The substrate-binding pocket of ζ -crystallin-like QORs is proposed to be close to the nicotinamide moiety of the NADPH cofactor (Pan et al., 2009; Thorn et al., 1995). Structural comparison revealed that the pocket entrance in human ζ -crystallin–NADPH

is relatively large (Fig. 5B) compared to yeast Zta1–NADPH (Fig. 5C) and *E. coli* QOR–NADPH (Fig. 5D). This size difference mainly resulted from the replacement of a single gated Arg residue in *E. coli* QOR (Arg263) and Zta1 (Arg270), to Gly268 in human ζ -crystallin. Furthermore, structure-based sequence alignment showed that the Arg is conserved in lower organisms but replaced by Gly in vertebrates (including *Branchiostoma lanceolatum*) (Fig. 5A). To explore the influence of the change in the ζ -crystallin–QORs, the R270G mutant was constructed and used in activity assays (Table S1). k_{cat} and k_{cat}/K_m towards both standard substrates increased, with k_{cat}^{NQ} and k_{cat}^{PQ} for R270G increased by 60–70%, whereas the K_m^{NQ} and K_m^{PQ} values were similar to wild-type. We propose that the replacement of Arg with Gly might results in the elevation of enzymatic activity throughout evolution, probably via enlarging the pocket entrance.

3.6. Putative mechanism for catalysis

Based on the docking results and enzyme assays, we propose the following catalytic mechanism for Zta1. The cofactor-binding pocket and the active site in the apo-enzyme are fairly open and

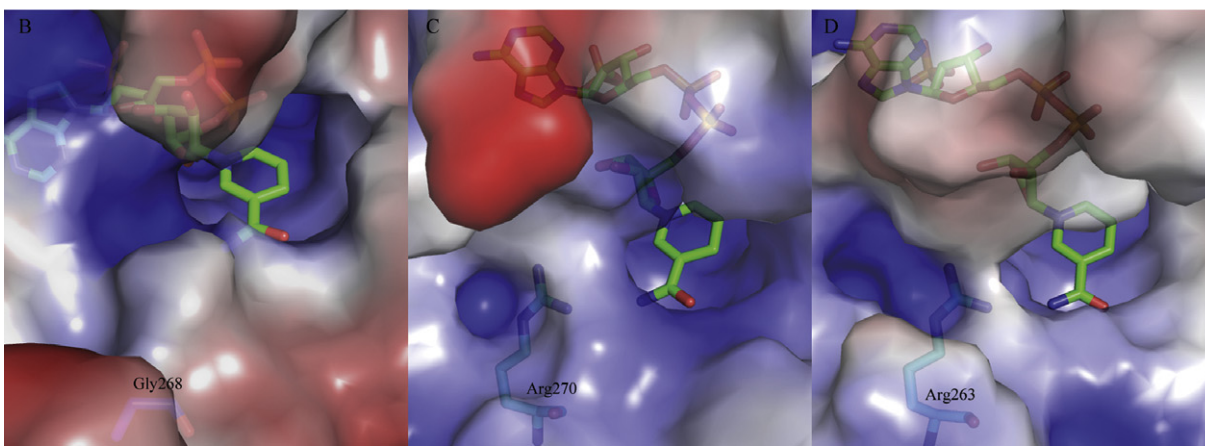
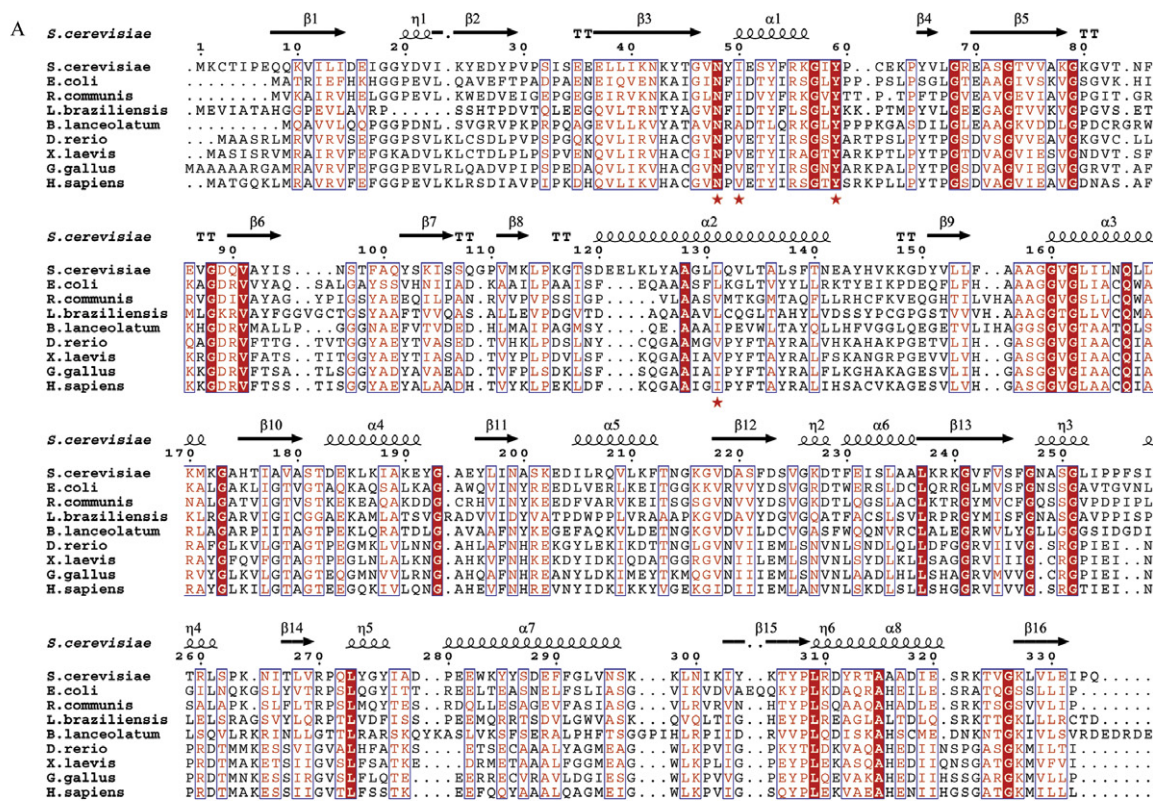


Fig. 5. Evolution of ζ -crystallin-like QORs. (A) Structure-based sequence alignment of ζ -crystallin-like QORs from *Escherichia coli* (ZP_07160882.1), *Saccharomyces cerevisiae* (NP_009602.1), *Ricinus communis* (XP_002510987.1), *Leishmania braziliensis* (XP_001561638.1), *Branchiostoma lanceolatum* (XP_002613985.1), *Danio rerio* (NP_001019546.1), *Xenopus laevis* (NP_001086430.1), *Gallus gallus* (NP_001073231.1) and *Homo sapiens* (NP_001880.21). Secondary structure elements of Zta1 (PDB code: 3QWA) are at the top. Residues involved in the substrate-binding site are marked with red stars, and the key residue at the entrance is marked with a blue triangle. Alignments were performed with *ClustalW* and *ESPrpt*. The entrance of the substrate-binding pocket of (B) human ζ -crystallin, (C) Zta1 and (D) *E. coli* QOR. NADPH is in green, and the key residues are in blue (human ζ -crystallin) and cyan (Zta1 and *E. coli* QOR). (For interpretation of the references to colour in this figure legend, the reader is referred to the web version of this article.)

relaxed. Upon NADPH binding, Domain I and II move towards each other, narrowing the interdomain cleft. At the same time, the residues around the active site assemble to form an ideal substrate-binding cavity. Quinone enters the pocket and is correctly positioned by the side chains of Asn48, Ile50, Tyr59, and Leu131, as well as the NADPH nicotinamide ring. In the holoenzyme, the active site is more shielded from solution than in the apo-form. Electron transfer occurs once the phenyl ring of quinone is aligned parallel to the nicotinamide ring via π - π stacking interactions. An increase in hydrophobicity around the positively charged nicotinamide group in the ternary enzyme-NADPH-substrate facilitates electron transfer from NADPH to substrate (Eklund

et al., 1981). Upon reduction of the quinone carbonyl group, the hydrogen bond between the side chain of Asn48 and *ortho*-quinone is broken. With the redox state change, the conformation of NADP⁺ also may change, accompanied by the opening of the interdomain cleft for the release of the product.

4. Conclusions

This work reports the structures of Zta1 and Zta1-NADPH complex, and reveals a noticeable induced fit upon NADPH binding. Computational simulation combined with site-directed mutagenesis

sis and enzymatic activity assays enable us to define the potential quinone-binding site of Zta1 and ζ -crystallin-like QORs. Furthermore, the replacement of Arg with Gly at the gate of the substrate-binding pocket might cause elevation of enzymatic activity of ζ -crystallin-like QORs from lower to higher organisms.

5. Accession numbers

Atomic coordinate and structure factor of Zta1apo-form and Zta1complexed with NADPH were deposited in the Protein Data Bank (<http://www.rcsb.org>) under the accession codes 3QWA and 3QWB, respectively.

Acknowledgments

We would like to thank Yang Du and Yong-Liang Jiang at USTC for the help on docking simulation. We thank the staffs at the Shanghai Synchrotron Radiation Facility for the data collection. We are grateful to all the developers of CCP4 Suit, ESPript, MolProbity and PyMOL. This work was supported by the National Natural Science Foundation of China (Program 30870490) and the Ministry of Science and Technology of China (Project 2006CB910202).

Appendix A. Supplementary data

Supplementary data associated with this article can be found, in the online version, at [doi:10.1016/j.jsb.2011.07.010](https://doi.org/10.1016/j.jsb.2011.07.010).

References

- Adams, P.D., Grosse-Kunstleve, R.W., Hung, L.W., Ioerger, T.R., McCoy, A.J., Moriarty, N.W., Read, R.J., Sacchettini, J.C., Sauter, N.K., Terwilliger, T.C., 2002. PHENIX: building new software for automated crystallographic structure determination. *Acta Crystallogr. D Biol. Crystallogr.* 58, 1948–1954.
- Bolton, J.L., Trush, M.A., Penning, T.M., Dryhurst, G., Monks, T.J., 2000. Role of quinones in toxicology. *Chem. Res. Toxicol.* 13, 135–160.
- Colonna-Cesari, F., Perahia, D., Karplus, M., Eklund, H., Braden, C.I., Tapia, O., 1986. Interdomain motion in liver alcohol dehydrogenase. Structural and energetic analysis of the hinge bending mode. *J. Biol. Chem.* 261, 15273–15280.
- Crosas, E., Porte, S., Moeini, A., Farres, J., Biosca, J.A., Pares, X., Fernandez, M.R., 2011. Novel alkenal/one reductase activity of yeast NADPH:quinone reductase Zta1p. Prospect of the functional role for the zeta-crystallin family. *Chem. Biol. Interact.*
- DeLano, W., 2002. The PyMOL Molecular Graphics System. DeLano Scientific, San Carlos, CA, USA.
- Dinkova-Kostova, L.T., Talalay, P., 2000. Persuasive evidence that quinone reductase type 1 (DT diaphorase) protects cells against the toxicity of electrophiles and reactive forms of oxygen. *Free Radic. Biol. Med.* 29, 231–240.
- Eklund, H., Samma, J.P., Wallen, L., Branden, C.I., Akeson, A., Jones, T.A., 1981. Structure of a triclinic ternary complex of horse liver alcohol dehydrogenase at 2.9 Å resolution. *J. Mol. Biol.* 146, 561–587.
- Emsley, P., Cowtan, K., 2004. Coot: model-building tools for molecular graphics. *Acta Crystallogr. D Biol. Crystallogr.* 60, 2126–2132.
- Fernandez, M.R., Porte, S., Crosas, E., Barbera, N., Farres, J., Biosca, J.A., Pares, X., 2007. Human and yeast zeta-crystallins bind AU-rich elements in RNA. *Cell. Mol. Life. Sci.* 64, 1419–1427.
- Garland, D., Rao, P.V., Del Corso, A., Mura, U., Zigler Jr., J.S., 1991. Zeta-Crystallin is a major protein in the lens of *Camelus dromedarius*. *Arch. Biochem. Biophys.* 285, 134–136.
- Goodsell, D.S., Morris, G.M., Olson, A.J., 1996. Automated docking of flexible ligands: applications of AutoDock. *J. Mol. Recognit.* 9, 1–5.
- Huang, Q.L., Russell, P., Stone, S.H., Zigler Jr., J.S., 1987. Zeta-crystallin, a novel lens protein from the guinea pig. *Curr. Eye Res.* 6, 725–732.
- Huey, R., Morris, G.M., Olson, A.J., Goodsell, D.S., 2007. A semiempirical free energy force field with charge-based desolvation. *J. Comput. Chem.* 28, 1145–1152.
- Jaiswal, A.K., 2000. Characterization and partial purification of microsomal NAD(P)H:quinone oxidoreductases. *Arch. Biochem. Biophys.* 375, 62–68.
- Li, R., Bianchet, M.A., Talalay, P., Amzel, L.M., 1995. The three-dimensional structure of NAD(P)H:quinone reductase, a flavoprotein involved in cancer chemoprotection and chemotherapy: mechanism of the two-electron reduction. *Proc. Natl. Acad. Sci. USA* 92, 8846–8850.
- Lovell, S.C., Davis, I.W., Arendall 3rd, W.B., de Bakker, P.I., Word, J.M., Prisant, M.G., Richardson, J.S., Richardson, D.C., 2003. Structure validation by Calpha geometry: phi, psi and Cbeta deviation. *Proteins* 50, 437–450.
- Maruyama, A., Kumagai, Y., Morikawa, K., Taguchi, K., Hayashi, H., Ohta, T., 2003. Oxidative-stress-inducible qorA encodes an NADPH-dependent quinone oxidoreductase catalysing a one-electron reduction in *Staphylococcus aureus*. *Microbiology* 149, 389–398.
- Monks, T.J., Jones, D.C., 2002. The metabolism and toxicity of quinones, quinonimines, quinone methides, and quinone-thioethers. *Curr. Drug Metab.* 3, 425–438.
- Morris, G.M., Goodsell, D.S., Halliday, R.S., Huey, R., Hart, W.E., Bewley, R.K., Olson, A.J., 1998. Automated docking using a Lamarckian genetic algorithm and an empirical binding free energy function. *J. Comput. Chem.* 19, 1639–1662.
- Murshudov, G.N., Vagin, A.A., Dodson, E.J., 1997. Refinement of macromolecular structures by the maximum-likelihood method. *Acta Crystallogr. D Biol. Crystallogr.* 53, 240–255.
- Nioi, P., Hayes, J.D., 2004. Contribution of NAD(P)H:quinone oxidoreductase 1 to protection against carcinogenesis, and regulation of its gene by the Nrf2 basic-region leucine zipper and the arylhydrocarbon receptor basic helix-loop-helix transcription factors. *Mutat. Res.-Fundam. Mol. Mech. Mutagen.* 555, 149–171.
- Oppermann, U., 2007. Carbonyl reductases: the complex relationships of mammalian carbonyl- and quinone-reducing enzymes and their role in physiology. *Annu. Rev. Pharmacol. Toxicol.* 47, 293–322.
- Otwinowski, Z., Minor, W., 1997. Processing of X-ray diffraction data collected in oscillation mode. *Macromol. Crystallogr. Pt. A* 276, 307–326.
- Pan, X., Zhang, H., Gao, Y., Li, M., Chang, W., 2009. Crystal structures of *Pseudomonas syringae* pv. tomato DC3000 quinone oxidoreductase and its complex with NADPH. *Biochem. Biophys. Res. Commun.* 390, 597–602.
- Porte, S., Crosas, E., Yakovtseva, E., Biosca, J.A., Farres, J., Fernandez, M.R., Pares, X., 2009a. MDR quinone oxidoreductases: the human and yeast zeta-crystallins. *Chem. Biol. Interact.* 178, 288–294.
- Porte, S., Valencia, E., Yakovtseva, E.A., Borrás, E., Shafiqat, N., Debreczeny, J.E., Pike, A.C., Oppermann, U., Farres, J., Fita, I., Pares, X., 2009b. Three-dimensional structure and enzymatic function of proapoptotic human p53-inducible quinone oxidoreductase PIG3. *J. Biol. Chem.* 284, 17194–17205.
- Porte, S., Moeini, A., Reche, I., Shafiqat, N., Oppermann, U., Farres, J., Pares, X., 2011. Kinetic and structural evidence of the alkenal/one reductase specificity of human zeta-crystallin. *Cell. Mol. Life Sci.* 68, 1065–1077.
- Prestera, T., Holtzclaw, W.D., Zhang, Y.S., Talalay, P., 1993. Chemical and molecular regulation of enzymes that detoxify carcinogens. *Proc. Natl. Acad. Sci. USA* 90, 2965–2969.
- Rao, P.V., Krishna, C.M., Zigler Jr., J.S., 1992. Identification and characterization of the enzymatic activity of zeta-crystallin from guinea pig lens. A novel NADPH:quinone oxidoreductase. *J. Biol. Chem.* 267, 96–102.
- Rao, S.T., Rossmann, M.G., 1973. Comparison of super-secondary structures in proteins. *J. Mol. Biol.* 76, 241–256.
- Shimomura, Y., Kakuta, Y., Fukuyama, K., 2003. Crystal structures of the quinone oxidoreductase from *Thermus thermophilus* HB8 and its complex with NADPH: implication for NADPH and substrate recognition. *J. Bacteriol.* 185, 4211–4218.
- Tang, A., Curthoys, N.P., 2001. Identification of zeta-crystallin/NADPH:quinone reductase as a renal glutaminase mRNA pH response element-binding protein. *J. Biol. Chem.* 276, 21375–21380.
- Thorn, J.M., Barton, J.D., Dixon, N.E., Ollis, D.L., Edwards, K.J., 1995. Crystal structure of *Escherichia coli* QOR quinone oxidoreductase complexed with NADPH. *J. Mol. Biol.* 249, 785–799.
- Vagin, A., Teplyakov, A., 1997. MOLREP: an automated program for molecular replacement. *J. Appl. Crystallogr.* 30, 1022–1025.
- Yagi, T., 1991. Bacterial NADH-quinone oxidoreductases. *J. Bioenerg. Biomembr.* 23, 211–225.